A&A 398, 949–957 (2003)
DOI: 10.1051/0004-6361:20021718

Astronomy & Astrophysics

New *UBVRI* color distributions in E-type galaxies

II. Central and mean metallicities⋆

T. P. Idiart[1,3], R. Michard[2], and J. A. de Freitas Pacheco[1]

[1] Observatoire de la Côte d'Azur, BP 4229, 06304 Nice Cedex 4, France
e-mail: pacheco@obs-nice.fr
[2] Observatoire de Paris, LERMA, 77 Av. Denfert-Rochereau, 75015, Paris, France
[3] Instituto de Astronomia, Geofísica e Ciências Atmosféricas Depto. de Astronomia, Universidade de São Paulo, Av. Miguel Stefano, 4200-CEP 04301-904, S. Paulo, SP-Brazil
e-mail: thais@iagusp.usp.br

Received 17 September 2001/ Accepted 8 November 2002

Abstract. Central and mean metallicities are calculated for a sample of 40 early-type galaxies, whose color gradients were reported in a previous paper (Idiart et al. 2002). The present color-metallicity calibration was derived from a grid of evolutionary models which fit the color-magnitude sequence of ellipticals in Coma and Virgo clusters. The mean metallicity gradient derived from our data is $(\Delta[\mathrm{Fe/H}]/\Delta \log r) = -0.26 \pm 0.08$ and the mean sample average metallicity is $< [\mathrm{Fe/H}] > = 0.01 \pm 0.11$ (rmsd). Central and mean metallicities are correlated with the central velocity dispersion, consistent with the interpretation by metallicity variations of the color-magnitude sequence and of color gradients. Age effects are also discussed, in particular concerning the interpretation of the Hβ line strength in those objects.

Key words. galaxies: ellipticals and lenticular, cD – galaxies: abundances

1. Introduction

The integrated properties of early-type galaxies are linked to the chemical and spectrophotometric evolution of their stellar populations: the integrated colors of ellipticals become redder as the luminosity increases (Visvanathan & Sandage 1977). On the other hand, the strength of the Mg_2 index also increases with the luminosity, and correlates well with the central velocity dispersion for E galaxies (Terlevich et al. 1981; Bender et al. 1993) or for bulges (Idiart et al. 1996). These relations can be understood if brighter galaxies have higher metallicities. This is perhaps not the whole story however: Worthey (1996) discusses the data for various line indices using his grid of *single stellar population* (SSP) models (Worthey 1994), and finds indications of an Age-Z trend. Trager et al. (2000) (TFWG) also use these SSP models to interpret the chemical history of local ellipticals, but they incorporate corrections for non-solar abundance ratios. This particular aspect of the index – metallicity calibration was first raised by Borges et al. (1995), who obtained fitting formulas for indices like Mg_2, NaD, ..., including the explicit dependence of the relative element abundance with respect to iron, in order to avoid the bias, present in any spectral library, introduced by the chemical history of our Galaxy. The deviations of E-galaxies populations from the solar composition are reviewed by Worthey (1998); Henry & Worthey (1999).

Using colors and spectral indices derived from *evolutionary models*, including gas inflow and outflow, Bressan et al. (1996) conclude that E-galaxies do not follow a pure sequence either of age or metallicity; while all are old objects (13–15 Gyr), some of them have continued to form stars for long periods. Kodama & Arimoto (1997) tried to solve the age-metallicity degeneracy by building up two model sequences (age and metallicity sequences), normalized to reproduce the CMR of ellipticals in the Coma cluster. They compared the evolution of both CMR sequences up to redshifts $z \sim 1$, and concluded that the age sequence deviates significantly from observations already at $z \sim 0.3$, supporting the view that the CMR results primarily from a metallicity variation with luminosity. A similar conclusion is reached by Tamura et al. (2000) from the analysis of ellipticals in the Hubble "deep-field", as well as by Saglia et al. (2000), who also study the evolution of color gradients with the redshift.

If these last studies favor the interpretation of the CMR as a "metallicity sequence", uncertainties still persists in the interpretation of color gradients across E-galaxies. Early-type galaxies tend to be redder in the central regions (Franx et al. 1989; Peletier et al. 1990; Goudfrooij et al. 1994;

Send offprint requests to: R. Michard,
e-mail: raymond.michard@obspm.fr

⋆ Based partially on data collected at the Observatory of Haute-Provence.

Michard 1998a, 1998b, 2000), probably due to the presence of a *negative* metallicity gradient along the radius. This interpretation is corroborated by spectroscopic observations, with generally *negative* line-strength gradients in ellipticals (Faber 1977; Davidge 1992; Carollo et al. 1993; Davies et al. 1993; Fisher et al. 1995), except Hβ, which displays a *positive* gradient in most of the cases. Broad-band color gradients are readily interpreted with SSP models (Peletier et al. 1990). The same is true for line spectrophotometric indices, like those defined by the Lick's team (see Faber et al. 1985). Recently, Kobayashi & Arimoto (1999) (KA99) used the Worthey's SSP models and a compilation of line-strength gradients from the literature, to compute mean metallicities for a sample of 80 E-galaxies. Evolutionary models have also been introduced in the discussion of spectrophotometric gradients by Tantalo et al. (1998), who found that the nuclear region of some E-galaxies are not only metal-rich but have also a stellar population younger than the outer zones, raising again the question of possible age differences among stellar populations along the radius.

Radial metallicity gradients can be explained by the dissipative collapse picture. The very first hydrodynamical calculations by Larson (1974, 1975) gave Δ[Fe/H]/$\Delta \log r$ ranging from -0.35 up to -1.0, while N-body simulations (Carlberg 1984) suggest values around -0.5. These predictions are "steeper" than those derived from colors and line strength gradients, which are typically about -0.3 dex per decade. However, E-galaxies formed in a pure merging picture should have a very flat gradient, since merging events tend to erase any pre-existing gradient (White 1980).

The conversion of color or line strength gradients into mean metallicities or/and mean population ages requires the use of high quality data. In the present work, central and mean metallicities are derived for a sample of 40 early-type galaxies, whose *UBVRI* colors and gradients were reported in a preceding paper (Idiart et al. 2002, hereafter Paper I). We believe that the present data have an accuracy adequate for our purposes, since special care has been taken to improve corrections due to residual background effects, the PSF far wings and "red halo" (for a detailed analysis of these effects, see also Michard 2002). Moreover, color gradients have been calculated in selected ranges, avoiding the central regions of some objects affected by dust. This procedure enables us to obtain by extrapolation reliable colors of the underlying stellar population in the center of the galaxy (see Paper I).

As detailed below, the color-metallicity calibration was derived from *evolutionary models* (de Freitas Pacheco 1996), which are expected to take into account the gradual chemical enrichment of the stellar populations.The upgrade of these models has not yet been fully described in a dedicated paper, so that Sect. 2 is devoted to a summary of their derivation, hopefully sufficient for an understanding of their use in the present contribution. In Sect. 3 we apply the models to calculations of the average and central metallicities from our color data. In Sect. 4 various tests of the validity of our results are presented.

A detailed discussion of our evolutionary models, involving various choices of the input parameters, and the corresponding comparisons with colors and other spectral indices, is outside the scope of this paper. A forthcoming paper will give more details, when the evolution of the spectrophotometric properties as a function of the redshift will be explored.

Often used notations

- r isophotal (or equivalent) radius. $r = (ab)^{1/2}$ for an ellipse of semi-axis a and b.
- Δ_{U-V} colour gradient in $U-V$. $\Delta_{U-V} = \mathrm{d}(U-V)/\mathrm{d}(\log r)$ and similar for other spectral indices.

2. The color-metallicity calibration

The calibration used in the present work was derived from a set of models of elliptical galaxies computed according to the assumptions described by de Freitas Pacheco (1996). These models are of the "one layer" type (Bressan et al. 1994). The star formation activity always begins at the same redshift: all galaxies have the same age, i.e. 15 Gyr. The star formation efficiency however, varies among models being an increasing function of galaxy mass. Furthermore, the IMF slope is slightly dependent on mass. The models of various masses accordingly develop stellar populations of different mean ages, chemical compositions and spectral properties.

Some important points in the derivation of these models are now given:

- The input parameters were chosen by an iterative procedure in order to reproduce the color-magnitude diagram, $U-V$ against M_V of ellipticals in Coma and Virgo (Bower et al. 1992a, 1992b), a procedure also employed by Kodama & Arimoto (1997) to compute the CMR at different redshifts. Compliance with a chosen CMR is an usual ingredient of evolutionary models without or with infall (Bressan et al. 1994; Tantalo et al. 1996) Fig. 1 compares the theoretical color-magnitude diagram with the used data;
- Due attention was given to the "contradiction" between the theoretical requirements for describing the CMR as a mass-metallicity relation on the one hand, and for avoiding the undue enhancement of Fe relative to α-elements which would result from "too many" SNe Ia on the other (see a recent discussion by Tantalo & Chiosi 2002). The usual "delayed-wind" picture (Matteucci 1994) can explain the observed CMR for ellipticals. However, since this model predicts that the star formation ceases later in more massive galaxies, not only the mean metallicity increases but also the relative contribution of SNe Ia, whose ejecta are iron-rich. As a consequence, the relative abundance of the α-elements decreases in the medium, producing a population mix with a decreasing < [Mg/Fe] > ratio, contrary to observations (Matteucci & Tornambè 1987; Matteucci et al. 1998; Worthey 1998). This problem can be solved either by assuming that the more massive E-galaxies have a higher star formation rate, or by assuming that such objects have flatter initial mass functions (Matteucci et al. 1998; Worthey 1998; Chiosi et al. 1998; Tantalo et al. 1998). In fact, we played with both possibilities. Not only higher star formation efficiencies for massive ellipticals are necessary to explain the CMR, but also flatter IMFs, if an adequate (?) representation of data in the Mg_2–<Fe> diagram is equally required;

Table 1. Model properties: The columns give respectively the model identification (1), the initial mass of the galaxy (2), the star formation efficiency (3), the exponent of the IMF (4), the mass fraction lost by the wind (5), the mean age (6), the mean metallicity (7) and the mean relative abundance ratio [Mg/Fe] (8) of the population mix.

Model (1)	M_0 ($M_\odot$) (2)	k (Gyr^{-1}) (3)	γ (4)	f_g (5)	τ_*(Gyr) (6)	< [Fe/H] > (7)	< [Mg/Fe] > (8)
1	2×10^{10}	0.445	2.27	0.201	12.5	−0.248	0.44
2	5×10^{10}	0.510	2.22	0.159	12.6	−0.103	0.47
3	2×10^{11}	0.630	2.14	0.110	12.7	+0.109	0.49
4	7×10^{11}	0.730	2.10	0.079	12.9	+0.213	0.49
5	2×10^{12}	0.835	2.06	0.059	13.0	+0.306	0.50

Table 2. Spectrophotometric properties: The columns give respectively the model $N0$. (1), the absolute magnitude in the V-band (2), the $U-V$, $B-V$, $B-R$, $V-I$ colors (3) to (6), the indices Mg_2 (7) and Hβ (8).

$N0$ (1)	M_v (2)	$U-V$ (3)	$B-V$ (4)	$B-R$ (5)	$V-I$ (6)	Mg_2 (7)	Hβ (8)
1	−18.29	1.192	0.909	1.51	1.28	0.237	2.04
2	−19.20	1.283	0.949	1.57	1.32	0.259	1.94
3	−20.55	1.424	1.007	1.66	1.38	0.286	1.77
4	−21.85	1.553	1.045	1.71	1.41	0.297	1.63
5	−22.92	1.668	1.076	1.75	1.43	0.305	1.52

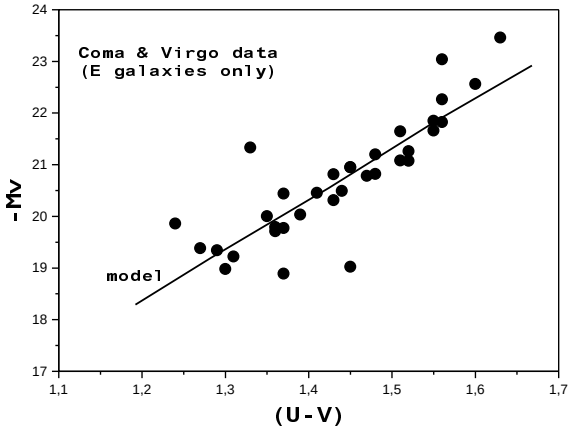

Fig. 1. Color-magnitude calibration: the solid line represents the grid of models whose parameters (see text) were adjusted to fit the sequence of data points on Coma and Virgo ellipticals.

– The evolutionary tracks of the Padova group were used in the computations, and the integrated properties of the stellar population could be derived in a self-consistent way, for any power-law representing the initial mass function (IMF);
– Fluxes in the filters U, B, V, R_c, I_c, K and corresponding colors were computed from the Padova tracks using transformations from bolometric magnitudes and effective temperatures by Vandenberg (1992). Using the fitting functions derived from the spectral library by Borges et al. (1995), our code computes the Lick indices Mg_2, < Fe > = $\frac{1}{2}$(Fe5270+Fe5335), Hβ, NaD and CaT. Note that the colors of the SSP used in our synthesis code were computed taking into account effects due to variations of the IMF. For the Lick indices, we adopted the calibrations by Borges et al. (1995), including also effects due to the IMF changes.

The main properties of these models are summarized in Table 1. The second, third and fourth columns are the input parameters, namely, the initial mass of the galaxy, the star formation efficiency k (we recall that the star formation rate is proportional to the gas mass, namely, $kM_g(t)$) and the adopted exponent of the IMF ($\gamma = 2.35$ for a Salpeter's law). Note that in the extreme case (model 5), the required IMF differs only by about 12% from the usual Salpeter's law.

The following four columns give respectively the mass fraction lost by the galaxy due to the galactic wind, the mean age, the mean metallicity and the mean <[Mg/Fe]> ratio of the stellar population mix. Note that the <[Mg/Fe]> ratio increases only slightly from the less massive to the most massive model. It does not reproduce the larger range advocated by Worthey (1998), although Matteucci et al. (1998) find the data unconclusive (see also Kuntschner et al. 2001). It is worth mentioning that our models, for a residual gas mass of about 0.07 of the total mass (typical of spirals like the Milky Way), predict [Mg/Fe] ≈ 0.10, for a mean population age of 8 Gyr.

In Table 2 are given some of the models spectrophotometric properties which will be used in the present paper.

3. Central and mean metallicities

3.1. Derivation of metallicities from colors

3.1.1. The $U-V$ color

We suppose now that a given ellipsoidal shell inside a galaxy, with an equivalent radius r is constituted by a population mix, with a mean age comparable to that of the whole star population of a model galaxy. If, in a first approximation, radial flows and diffusion of stars from one shell to another are neglected, then each shell can be associated to a "one-zone galaxy", characterized by a mean metallicity which reflects the consequences of the star formation activity in this zone. If the observed color gradient is a consequence of a metallicity gradient throughout the galaxy, then it is possible to derive an expression for the latter, using actual data for the former and a theoretical color-metallicity calibration. In the present computations, we decided to use essentially the $U-V$ color for two reasons: on the one hand, its gradient is large enough to be measured with an

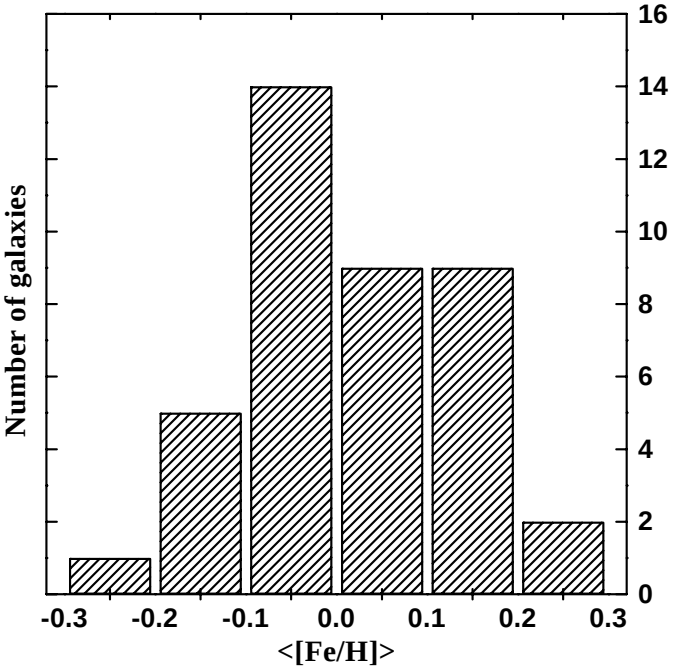

Fig. 2. Distribution of mean metallicities derived from color gradients.

accuracy adequate for our purposes; on the other, our models have been constrained to agree with the $U-V$–luminosity observed relation (Sect. 2).

In a first approximation, the variation of the $U-V$ color as a function of the radius is given by

$$U - V = (U - V)_0 + \Delta_{U-V} \cdot \log(r/r_0) \quad (1)$$

where $(U - V)_0$ is the color at the reference radius r_0 and Δ_{U-V} is the corresponding color gradient. These parameters are given in Paper I, for objects included in our sample. From Tables 1 and 2, one obtains a color-metallicity calibration given by

$$[\mathrm{Fe/H}] = -1.600 + 1.162 \cdot (U - V). \quad (2)$$

These two equations can be combined and one obtains

$$[\mathrm{Fe/H}] = [\mathrm{Fe/H}]_0 + \Delta_{[\mathrm{Fe/H}]} \cdot \log(r/r_0) \quad (3)$$

where $[\mathrm{Fe/H}]_0 = -1.600 + 1.162 \cdot (U - V)_0$ is the metallicity at the reference radius, and the resulting metallicity gradient is $\Delta_{[\mathrm{Fe/H}]} = 1.162 \cdot \Delta_{U-V}$. It is worth mentioning that from our data, the sample average gradient is $\Delta_{U-V} = -0.228 \pm 0.068$ (rmsd), which is equivalent to a mean metallicity gradient $\Delta_{[\mathrm{Fe/H}]} = -0.26 \pm 0.08$.

In order to compute the mean metallicity of the galaxy, the luminous weight of each shell must be introduced. Since the mass-to-luminosity ratio is also derived for each model of galaxy, it is also possible to compute an average metallicity weighted by the mass of the shell. Differences between both procedures are small, in agreement with other authors who have performed similar calculations (Yoshii & Arimoto 1987; Gibson 1997). Here the light weighted average is adopted since this definition corresponds better to what is observed. We assume that the light distribution along the radius can be represented by a de Vaucouleurs' law, namely,

$$I(r) = I_0 \mathrm{e}^{-\beta r^{1/4}}. \quad (4)$$

In this equation, the parameter I_0 is chosen adequately to normalize the light intensity in the interval r_1, r_2 and the parameter β is related to the effective radius (half-light) R_{eff} of the galaxy by $\beta = (3453/R_{\mathrm{eff}})^{1/4}$. The effective radius ($B$ color) used in our computations is given in the fifth column of Table 3 (in arcsec) and was obtained from the RC3, readable directly from the CDS-Strasbourg. Under these conditions, the mean metallicity is

$$< [\mathrm{Fe/H}] > = \log \int_{r_1}^{r_2} 2\pi r I(r) 10^{[\mathrm{Fe/H}]} \mathrm{d}r \quad (5)$$

where the integration limits were taken respectively equal to $r_1 = 1.5''$ and $r_2 = 2R_{\mathrm{eff}}$. The resulting mean metallicities are given in the second column of Table 3 and the third column gives the central metallicity computed at r_1 (see Paper I concerning the adopted definitions of central colors).

3.1.2. The case of other colors

From the colors for each model collected in Table 2, linear relations similar to (2) are readily derived. The slopes are

$$\Delta_{[\mathrm{Fe/H}]} = 3.33 \cdot \Delta_{B-V},$$
$$\Delta_{[\mathrm{Fe/H}]} = 2.30 \cdot \Delta_{B-R},$$
$$\Delta_{[\mathrm{Fe/H}]} = 3.63 \cdot \Delta_{V-I}.$$

These colors are two or three times less sensitive to metallicity than $U-V$. Considering the distributions of color gradients given in Paper I, the mean [Fe/H] gradients are estimated to be 0.24 from $B-V$, 0.22 from $B-R$ or $V-I$, *in fair agreement with the value of 0.26 derived from $U-V$ gradients.* The same is true of the range (and dispersion) of [Fe/H] values, central or average, trough our sample of galaxies (see below). Unfortunately there is no such agreement as regards the mean metallicities. The calculated $B-V$, $B-R$ and $V-I$ of the models are too red for their assumed $U-V$: these deviations from the observed color-color relations translate into large differences in estimated [Fe/H], since they are multiplied by the slope coefficients given above. The mean [Fe/H] values calculated from $B-V$ are thus 0.25 dex smaller than from $U-V$, a discrepancy reaching 0.41 for $B-R$, the $V-I$ being intermediate. In this connection note that uncertainties in the calculated colors of old stellar populations have been discussed by Charlot et al. (1996). In the following we accept as reliable the [Fe/H] values derived from the $U-V$ data, because of the built-in property of our models, i.e. to agree with the CMR as plotted from observed and calculated $U-V$ colors (see Fig. 1).

3.2. Metallicities distribution

– *Mean metallicities derived from colors*, according to Table 3, are in the range $-0.21 < [\mathrm{Fe/H}] < +0.24$, corresponding respectively to NGC 3377 and NGC 4649. Figure 2 shows the mean metallicity distribution derived for our sample, characterized by an average value (and dispersion) of $< [\mathrm{Fe/H}] > = 0.01 \pm 0.11$. Central values are about 0.28 dex higher with nearly the same dispersion.

Table 3. Central and mean metallicities: The columns give respectively the galaxy identification (1), the mean metallicity (2), the central metallicity from colors (3), the central metallicity from Mg_2 indices (4), the effective radius in arcsec (5) and the log of the central velocity dispersion (6).

NGC (1)	< [Fe/H] > (2)	$([Fe/H]_c)_{uv}$ (3)	$([Fe/H]_c)_{Mg_2}$ (4)	R_{eff} (5)	$\log\sigma_0$ (km s^{-1}) (6)
2768	+0.046	+0.263	+0.041	64.1	2.277
2974	+0.082	+0.403	+0.242	24.4	2.359
3115	+0.126	+0.399	+0.314	32.2	2.424
3193	+0.032	+0.297	+0.202	26.7	2.313
3377	−0.211	+0.055	+0.000	34.4	2.135
3379	+0.136	+0.322	+0.306	35.3	2.313
3605	−0.170	+0.061	−0.457	21.2	1.995
3607	+0.008	+0.238	+0.266	43.4	2.336
3608	−0.007	+0.287	+0.338	33.7	2.310
3610	−0.109	+0.070	−0.104	15.4	2.215
3613	+0.017	+0.284	+0.073	27.4	2.336
3640	−0.018	+0.172	−0.055	32.2	2.267
3872	+0.120	+0.304	+0.386	18.1	2.408
4125	+0.030	+0.378	+0.202	58.5	2.380
4261	+0.222	+0.530	+0.483	36.1	2.500
4278	−0.096	+0.183	+0.169	34.4	2.402
4283	−0.003	+0.280	−0.015	12.5	2.123
4365	+0.152	+0.392	+0.410	49.8	2.429
4374	+0.048	+0.255	+0.282	50.1	2.473
4387	−0.042	+0.097	−0.240	15.7	2.069
4406	−0.008	+0.318	+0.330	94.9	2.407
4472	+0.180	+0.473	+0.290	104.0	2.484
4473	−0.025	+0.221	+0.274	26.1	2.280
4478	−0.145	+0.120	−0.135	13.4	2.183
4486	+0.125	+0.538	+0.403	94.9	2.545
4494	−0.071	+0.149	+0.041	48.7	2.199
4550	−0.167	+0.195	–	15.0	1.903
4551	+0.030	+0.154	−0.047	13.1	2.067
4552	+0.135	+0.412	+0.435	29.3	2.422
4564	−0.035	+0.296	+0.411	19.8	2.225
4621	+0.102	+0.425	+0.467	40.5	2.389
4636	−0.010	+0.436	+0.330	88.5	2.325
4649	+0.240	+0.500	+0.547	68.7	2.535
5322	−0.071	+0.179	+0.049	33.7	2.380
5576	−0.137	+0.068	−0.135	18.1	2.291
5813	+0.028	+0.201	+0.306	57.2	2.377
5831	−0.070	+0.144	+0.153	25.5	2.164
5846	+0.196	+0.458	+0.410	62.7	2.398
5866	−0.094	+0.262	–	40.5	2.153
5982	−0.011	+0.174	+0.210	23.8	2.399

This relatively narrow metallicity range agrees with the results by Gonzáles & Gorgas (1996) and TFWG. The latter determine ages and metallicities from a set of 3 line indices, taking into account non-solar chemical compositions: the average of their "central" metallicities for 12 objects in common with our sample (considering their favoured Model 4) roughly agrees with our values from the $U-V$ color, respectively 0.22 with $\sigma = 0.14$ for them, instead of 0.31 with $\sigma = 0.16$ for us. Part of the difference comes from the fact that we use colors at $r = 1.5''$ while they use indices averaged within $r = R_{eff}/8$. In fact, replacing our "central colors" by values integrated within $r = R_{eff}/8$ we recover a mean of 0.265 with $\sigma = 0.13$.

In KA99 mean metallicities are derived from line indices and their gradients, no allowance being made for non-solar compositions. The quoted interval is −0.8 to +0.3. The mean sample value for 20 objects with <[Fe/H]> measured from Mg_2 or Mg_b is −0.13 with $\sigma = 0.22$ that is 0.14 lower than our result, and with a larger dispersion. Note that in KA99, metallicities estimated from the <Fe> index are much lower than from the Mg indices, possibly due to the depletion of iron in old stellar populations discussed by

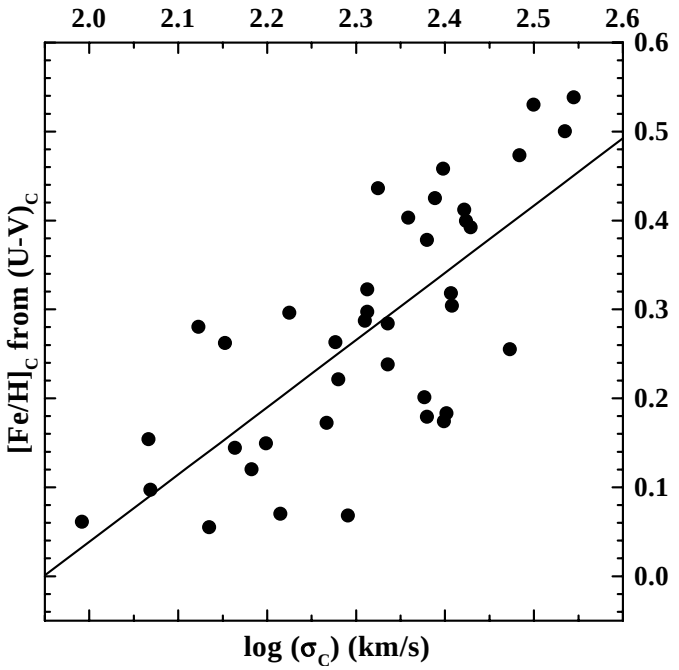

Fig. 3. Central metallicities derived from central colors, as a function of central dispersion velocities.

TFWG. This systematic difference also explains part of the large range of mean metallicities in KA99;

– *The well known Faber & Jackson (1976) relation*, between the luminosity (mass) and the central velocity dispersion, can be translated into a metallicity – σ_0 relation. In Fig. 3 we plot central metallicities *derived from the U−V colors* against central velocity dispersions. These quantities are clearly correlated and a least-squares fit gives:

$$[\mathrm{Fe/H}]_\mathrm{C} = -1.457 + 0.715 \cdot \log \sigma_\mathrm{C} \pm 0.097 \qquad (6)$$

with a correlation coefficient of 0.74. A correlation of similar robustness is found if mean, instead of central, metallicities are used, reinforcing the idea that the mass-metallicity relation of ellipticals holds for the whole stellar population and not only for the central regions. The dispersion in the correlation diagram of Fig. 3 is larger than implied by observational errors on colors and velocity dispersions: this results from cosmic scatter in the colors of E-galaxies in small groups or isolated. For instance, the most deviating data point at $\log \sigma_\mathrm{C} = 2.29$ and [Fe/H] = 0.07 corresponds to NGC 5576. This object deviates by 0.11 from the CMR in $U-V$ according to Schweizer & Seitzer (1992);

– *How would these results be modified by using SSP models?* The integrated color of a given SSP depends on the total metallicity Z, and thus systems with nonsolar abundance ratios may have different iron content for the same Z. Therefore, the conversion of [Fe/H] into Z (and vice versa) necessarily requires the knowledge of abundance ratios at the moment the system forms out of the interstellar medium. In our multi-population approach, since the time evolution of iron and other elements are followed, the integrated properties of the galaxy can be calculated self-consistently. Having in mind these problems, an SSP with an age and metallicity equal to the mean values of the stellar population of a galaxy will be slightly *redder*. For instance, a globular cluster with parameters comparable to our galaxy model 1 would have a color $U-V \approx 1.33$ instead of 1.19. Therefore, for a given color (and age), the use of SSPs for the calibration will lead to underestimates of the metallicity.

4. Discussion

In order to check the above derived metallicities and the internal consistency of the series of population models used for the calibration, we now consider the line indices.

1. *Comparison with metallicities from the Mg_2 index.*
We have computed central metallicities using the Mg_2 index, whose central values were taken from Davies et al. (1987). The relation [Fe/H]–Mg_2 can be obtained from the results given in Tables 1 and 2, namely

$$[\mathrm{Fe/H}] = -2.17 + 8.04 \cdot \mathrm{Mg_2}. \qquad (7)$$

It should be emphasized that this calibration was obtained in the framework of models constituted by a population mix with ages ranging from 12 to 13 Gyr (the more luminous galaxies have a population mix slightly older) and *non-solar* abundances. Central metallicities computed from this equation are given in the fourth column of Table 3. Incidentally, NGC 4486 has a low measured central Mg_2 index, but the profile shows a central drop probably produced by "dilution" of the stellar continuum (see, for instance, Terlevich et al. 1990) caused by the central blue object being associated with the optical jet. We have adopted for this galaxy a central value $Mg_2 = 0.32$, obtained from an extrapolation of the radial profile by Davidge (1992), when computing the central metallicity.
Figure 4 compares *central metallicities* resulting from $U-V$ colors with those resulting from Mg_2 line strengths. The good correlation between both determinations was expected (correlation coefficient equal to 0.81), since a robust correlation exists between the central $U-V$ colors and the central Mg_2 indices (Paper I). The mean sample difference is $[\mathrm{Fe/H}]_{U-V} - [\mathrm{Fe/H}]_{\mathrm{Mg_2}} = 0.076 \pm 0.120$ (rmsd), indicating a rather small systematic difference. The dispersion of about 0.12 dex could result largely from observational errors: indeed, with the calibration adopted (Eq. (7)), an error of 0.015 in Mg_2 translates into an error equal to the quoted dispersion. On the other hand, the slope of the correlation deviates clearly from the expected one of unity. The [Fe/H] for faint galaxies as derived from Mg_2 tend to be too low, as compared to the values obtained from $U-V$: the worst case is NGC 3605 (already with a rather low measured Mg_2 index). This systematic disagreement is somehow related to the calibration procedure summarized in Eqs. (2) and (6).
The comparison of our results with *average metallicities* derived from line strength gradients is more uncertain, since only 13 galaxies in our sample have measured Mg_2 gradients. Average metallicities were computed for these 13 galaxies, using the same procedure as above,

and Mg_2 index gradients from KA99. The mean difference between color and index metallicities is $< [Fe/H]_{U-V} > - < [Fe/H] >_{Mg_2} = +0.13 \pm 0.14$ (rmsd). The off-set as well as the dispersion are comparable to the values found in the analysis of central metallicities.

2. *The Mg_2 gradient* can be predicted from the Δ_{U-V} colour gradient and the calibration relations (2) and (6). The result is $\Delta_{Mg_2} \approx -0.032$ which should be compared to the mean sample value derived from the compilation in KA99, namely $\Delta_{Mg_2} = -0.052 \pm 0.019$ (rmsd). Only 13 objects in common between KA99 and our sample are used in this comparison, but the distribution for the complete KA99 sample is practically the same. The difference between the predicted and observed mean gradients is clearly larger than allowed by observational errors, and may reflect calibration problems, i.e. inaccuracies in the relations between various colors and spectral indices. The source of the discrepancy is clearly the same as found above in comparing the distributions of central metallicities in our sample of objects.
3. *If the Hβ index is considered*, do we still get a consistent picture? This index is mainly sensitive to the stellar temperature and hence to age effects, but a weak dependence on metallicity was found by Idiart & de Freitas Pacheco (1995) from the analysis of stars included in their spectral library, the basis of our population synthesis code. Our calibration procedure assumes that the population mix throughout E-galaxies has a small age spread. Variations of the star formation efficiency along the radius introduce a metallicity gradient and consequently radial effects on the blanketing, which should reduce the Hβ strength in the inner regions. In fact, most ellipticals display a flat or a positive gradient in Hβ, qualitatively consistent with expectations. From a quantitative point of view, the Hβ gradient can be predicted from the $U-V$ colour gradient and the slope of the Hβ–$(U-V)$ relation: from Table 2, this is equal to -1.105. Combining this with the mean sample gradient in the $U-V$ color given in the previous section, the predicted mean gradient of the Hβ index is approximately +0.25. This is compatible with the distribution of $\Delta_{H\beta}$ compiled in KA99, but the test is not stringent at all. Indeed the complete distribution has a mean of 0.18 ± 0.37(rmsd) for 45 objects; the subsample of 27 objects from Gonzàles observations gives 0.10 ± 0.26(rmsd), while the data from other observers (18 objects) lead to a mean of 0.30 ± 0.47(rmsd).
   Using a linear relation between the $U-V$ color and the Hβ index readily derived from Table 2, we can *predict* the latter from the observed color and compare the predicted values to the observed ones. For this comparison, we compiled near central Hβ index values for 33 galaxies of our sample, using the Lick/IDS data (Trager et al. 1998) and less extended samples by Gonzalez (1993), Davies et al. (1993), Kuntschner et al. (2001). For several objects there are several available measurements: this leads to a rather pessimistic view of the quality of the data, eventually polluted by emission in the Balmer line (corrected or not in the various sources). For instance, the measurements for NGC 4374 range from Hβ = 0.78 to 1.55. The relation between the predicted and observed Hβ indices is shown in Fig. 5 (the point for NGC 2974 has been discarded). The correlation is significant, with a coefficient $\rho = 0.50$. To our dismay, the slope clearly deviates from unity. Calling x and y the predicted and observed Hβ values respectively, we find the *impartial* regression $y = 2.04 \pm .23x - 1.68 \pm 0.04$ with $\sigma = 0.23$. In this calculation, each data point is weighted by the number of averaged measurements. We have repeated this comparison with a set of observed and calculated Hβ indices within an aperture of $r = R_{\rm eff}/8$: the data for 17 objects are from TFGW and from Kuntschner et al. The results are in fair agreement with the above, with a somewhat smaller dispersion of $\sigma = 0.19$ around an impartial regression of slope 1.78 ± 0.12, and with $\rho = 0.54$. Kuntschner et al. have compared their Hβ indices with previous data. We have completed this exercice, and got the σ-values of differences between 5 pairs of data-sources for the same galaxies: these vary from 0.16 (Gonzàles against Kuntschner et al.) to 0.28 (Lick/IDS against Kuntschner et al.). These values are of the same order of magnitude as the dispersions of residuals in the above regressions of predicted against observed Hβ indices: observational errors thus dominate these residuals.
   Altogether, the present check suggests that our evolutive models are able to represent the Hβ indices, at least in a first approximation, without introducing large ad hoc age differences between E-galaxies populations. This does not preclude some modifications of the primeval stellar populations in a minority of E-galaxies by the later accretion (or formation) of younger stars. This should result in *coherent changes* of both colors and line indices. TFWG give ages of circa 3–4 Gyr to such objects as NGC 3377 and 5831, but $U-V$ colors (measured in the same aperture) do not show the corresponding expected blueing.
   It is worth mentioning that effects other than age, may affect the Hβ strength. De Freitas Pacheco & Barbuy (1995) and de Freitas Pacheco (1997b) have shown that the Hβ strength in globular clusters depends on the horizontal branch morphology. Globular clusters with extended blue tails have larger Hβ indices. These clusters have also dense cores and the blue tails could be a consequence of dynamical effects on stellar evolution (Fusi-Pecci et al. 1993). These effects might contribute to mask the properties of the general stellar population.

5. Conclusions

– From color gradient data presented in Paper I and a color – metallicity calibration described in this work (Sect. 2), we derived a mean metallicity gradient for ellipticals $\Delta[Fe/H] = -0.26 \pm 0.08$. We calculated central and mean metallicities from the $U-V$ colors for 40 early-type objects. Our analysis indicates that ellipticals have mean metallicities of about the solar value, but some objects may have near center values as high as three times solar (NGC 4261, NGC 4486, NGC 4649 are examples).
– The derived mean and central metallicities are correlated with central velocity dispersions, an expected result if the CMR is essentially a metallicity sequence.

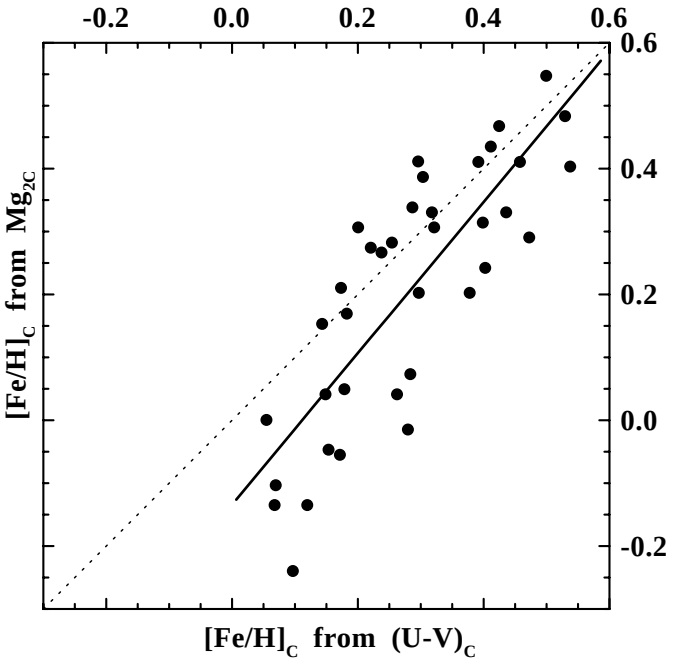

Fig. 4. Comparison between central metallicities derived from colors and line strength indices (Mg_2). Full line: calculated regression $Y = 1.2 \pm .14\,X + 0.13 \pm .05$. Dotted line $Y = X$.

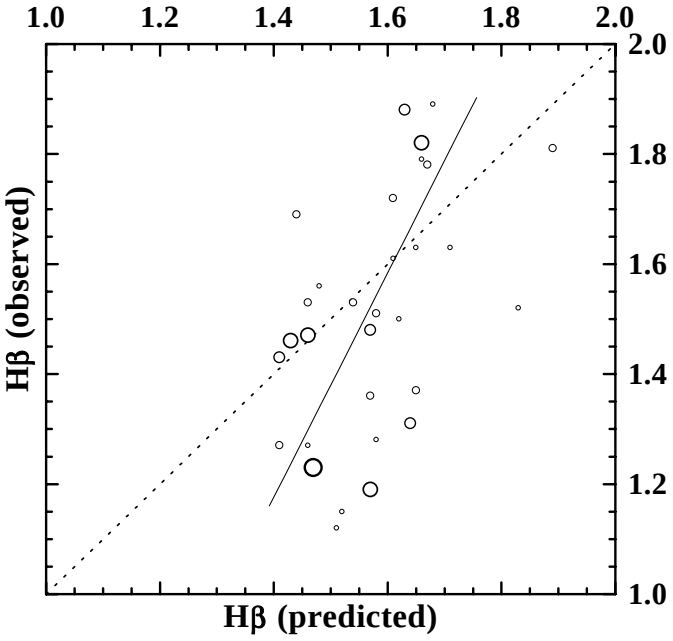

Fig. 5. Correlation between near center Hβ indices predicted from our $U-V$ colors (abscissae) and compiled observations (ordinates). The size of the symbols increases with the number of measurements averaged to define each observed index. Coefficient of correlation $\rho = 0.50$. Full line: regression of slope d(Obs)/d(Pred) ≈ 2.

– On the other hand we calculated the central and mean metallicities from the Mg_2 index and an index–metallicity calibration derived from the same set of population models. The results appear to be in reasonable agreement (Fig. 4), although a systematic difference in the distributions requires further study. Similarly, there are non trivial differences between the observed Mg_2 gradients and the values predicted from the $U-V$ gradients.

– We have predicted Hβ indices, using the metallicities derived from the $U-V$ colors plus our evolutive models, and compared these with observed data. Predicted and observed values for 32 galaxies have nearly the same mean and are reasonably correlated, but the slope of the regression is not unity, a systematic effect which requires further study. It appears that our grid of model galaxies, with a unique age of 15 Gyr, is roughly consistent with this set of data. This is at variance with the interpretation in terms of SSP with large age variations.

Acknowledgements. TPI acknowledges a Fapesp pos-doc fellowship No. 97/13083-7.

References

Borges, A. C., Idiart, T. P., de Freitas Pacheco, J. A., & Thévenin, F. 1995, AJ, 110, 2408
Bower, R. G., Lucey, J. R., & Ellis, R. S. 1992a, MNRAS, 254, 589
Bower, R. G., Lucey, J. R., & Ellis, R. S. 1992b, MNRAS, 254, 601
Bressan, A., Chiosi, C., Fagotto, F. 1994, A&AS, 94, 63
Bressan, A., Chiosi, C., & Tantalo, R. 1996, A&A, 311, 425
Carlberg, R. G. 1984, ApJ, 286, 403
Carollo, C. M., Danziger, I. J., & Buson, L. 1993, MNRAS, 2665, 553
Charlot, S., Worthey, G., & Bressan, A. 1996, ApJ, 457, 625
Chiosi, C., Bressan, A., Portinari, L., & Tantalo, R. 1998, A&A, 339, 355
Davies, R. L., Burstein, D., Dressler, A., et al. 1987, ApJS, 64, 581
Davies, R. L., Sadler, E. M., & Peletier, R. F. 1993, MNRAS, 262, 650
Davidge, T. J. 1992, AJ, 103, 1512
de Freitas Pacheco, J. A., & Barbuy, B. 1995, A&A, 302, 718
de Freitas Pacheco, J. A. 1996, Rev. Mex. Astron. Astrofis., Conf. Ser., 4, 51
de Freitas Pacheco, J. A. 1997a, A&A, 319, 394
de Freitas Pacheco, J. A. 1997b in Abundance Profiles: Diagnostic Tools for Galaxy History, ed. D. Friedli, M. Edmunds, C. Robert, & L. Drissen, ASP Conf. Ser., 147, 205
de Freitas Pacheco, J. A., Barbuy, B., & Idiart, T. P. 1998, A&A, 332, 19
Faber, S. M., & Jackson, R. E. 1976, ApJ, 204, 668
Faber, S. M. 1977, in The Evolution of Galaxies and Stellar Populations, ed. B. M. Tinsley, & R. B. Larson (Yale University Press), 157
Faber, S. M., Friel, E. D., Burstein, D., & Gaskell, C. M. 1985, ApJS, 57, 711
Fisher, D., Franx, M., & Illingworth, G. 1995, ApJ, 448, 119
Franx, M., Illingworth, G., & Heckman, T. 1989, AJ, 98, 538
Fusi-Pecci, F., Ferraro, F. R., Bellazini, M., et al. 1993, AJ, 105, 1145
Gibson, B. K. 1997, MNRAS, 290, 471
Goudfrooij, P., Hansen, L., Jorgensen, H. E., et al. 1994, A&AS, 104, 179
Gonzáles, J. J. 1993, Ph.D. Thesis, Univ. of California
Gonzáles, J. J., & Gorgas, J. 1996, in Fresh Views of Elliptical Galaxies, ed. A. Buzzoni, A. Renzini, & A. Serrano, ASP Conf. Ser., 86, 225
Henry, R. B. C., & Worthey, G. 1999, PASP, 111, 919
Idiart, T. P., & de Freitas Pacheco, J. A. 1995, AJ, 109, 2218
Idiart, T. P., de Freitas Pacheco, J. A., & Costa, R. D. D. 1996, AJ, 112, 254

Idiart, T. P., Michard, R., & de Freitas Pacheco, J. A. 2002, A&A, 383, 30 (Paper I)
Kodama, T., & Arimoto, N. 1997, A&A, 320, 41
Kobayashi, C., & Arimoto, N. 1999, ApJ, 527, 573 (KA99)
Kuntschner, H., Lucey, J. R., Smith, R. J., Hudson, M. J., & Davies, R. L. 2001, MNRAS, 323, 615
Larson, R. B. 1974, MNRAS, 166, 585
Larson, R. B. 1975, MNRAS, 173, 671
Matteucci, F., & Tornambè, A. 1987, A&A, 185, 51
Matteucci, F. 1994, A&A, 288, 57
Matteucci, F., Ponzone, R., & Gibson, B. K. 1998, A&A, 335, 855
Michard, R. 1998a, A&A, 334, 453
Michard, R. 1998b, A&A, 335, 479
Michard, R. 2000, A&A, 360, 85
Michard, R. 2002, A&A, 384, 763
Peletier, R. F., Davies, R. L., Illingworth, G., Davies, L., & Cawson, M. 1990, AJ, 100, 1091
Saglia, R. P., Maraston, C., Greggio, L., Bender, R., & Ziegler, B. 2000, A&A, 360, 911
Schweizer, F. & Seitzer, P. 1992, AJ, 104, 1039
Tamura, N., Kobayashi, C., Arimoto, N., Kodama, T., & Ohta, K. 2000, AJ, 119, 2134
Tantalo, R., Chiosi, C., Bressan, A., & Fagotto, F. 1996, A&A, 311, 361
Tantalo, R., Chiosi, C., & Bressan, A. 1998, A&A, 333, 419
Tantalo, R., & Chiosi, C. 2002, A&A, 388, 396
Terlevich, R., Davies, R. L., Faber, S. M., & Burstein, D. 1981, MNRAS, 196, 381
Terlevich, E., Díaz, A. I., & Terlevich, R. 1990, MNRAS, 242, 271
Trager, S. C., Faber, S. M., Worthey, G., & Gonzáles, J. J. 2000, AJ, 119, 1645 (TFWG)
Vandenberg, D. A. 1992, ApJ, 391, 685
Visvanathan, N., & Sandage, A. 1977, ApJ, 216, 214
White, S. D. 1980, MNRAS, 191, 1P
Worthey, G. 1994, ApJS, 95, 107
Worthey, G. 1996, in Fresh Views of Elliptical Galaxies, ed. A. Buzzoni, A. Renzini, & A. Serrano, ASP Conf. Ser., 86, 203
Worthey, G. 1998, PASP, 110, 888
Yoshii, Y., & Arimoto, N. 1987, A&A, 188, 13